Marine Structures 28 (2012) 86–100

Contents lists available at SciVerse ScienceDirect

Marine Structures

journal homepage: www.elsevier.com/locate/marstruc

Increased crashworthiness due to arctic conditions – The influence of sub-zero temperature

Sören Ehlers [a,*], Erling Østby [b]

[a] Dept. of Marine Technology, Norwegian University of Science and Technology, Otto Nielsens vei 10, 7491 Trondheim, Norway
[b] SINTEF, Materials and Chemistry, Trondheim, Norway

ARTICLE INFO

Article history:
Received 22 December 2011
Received in revised form 13 March 2012
Accepted 5 May 2012

Keywords:
Arctic conditions
Quasi-static and dynamic collision simulations
Material modelling
Cold-climate
Failure strain

ABSTRACT

Offshore activities and shipping in arctic regions increased significantly in the past decade due to the expected natural resources and due to the upcoming advantages of the northern sea route. Hence, structural solutions used in arctic conditions need to resist the low temperatures at an adequate safety level. Therefore, this paper analyses the collision resistance of ships exposed to sub-zero temperature (SZT). Further, it assesses the influence of the material properties for 0, −30, −60 and −90 °C of typical shipbuilding steel. Thereby, the theoretical influence of SZT on the collision force will be presented as well as the potential gain from specially selected materials for SZT, arctic materials, compared to standard materials, both with and without the presence of rupture. As a result, the potential increase in crashworthiness of structures under SZT will be presented and thereby a contribution to safe arctic operations and transport.

1. Introduction

Offshore activities and shipping in arctic regions increased significantly in the past decade due to the expected natural resources in the range of 13% of the world's undiscovered oil and gas and due to the upcoming advantages of the northern sea route (NSR). Furthermore, the global climate change continues to increase this marine transport in the Arctic Sea as a result of decreasing ice extends. Less ice provides new opportunities for shipping, leading to more intense and rapid development of arctic-

* Corresponding author. Tel.: +47 73 59 5596, +47 91 89 7748 (mobile); fax: +47 73 59 5697.
E-mail address: soren.ehlers@ntnu.no (S. Ehlers).

0951-8339/$ – see front matter © 2012 Elsevier Ltd. All rights reserved.
doi:10.1016/j.marstruc.2012.05.004

related technologies. DNV [1] expects 480 container ship trans-arctic voyages annually for 2030. Therefore, arctic transport and operations will continuously subject structures to harsh environmental conditions, respectively sub-zero temperatures (SZT) – thus structural solutions and materials need to be able to cope with this cold-climate on a safe level.

Hence, ships need to be able to withstand low temperatures and ice covered waters. Therefore, ice class certificates issued by classification societies (e.g. according to Finish-Swedish ice rules) reflect the ships' level of ice capability and are required in order to be admitted into ice covered waters or particular regions in seasons that have a certain probability of ice occurrence. However, accidental events, such as ship collisions under SZT are not addressed by these regulations even though they account for about 20 per cent of all serious accidents (IMO [2–6]). Hence they present a significant risk for the maritime transport environment, which is especially vulnerable in the high north. In conclusion, the scenario of a "black" ice bear due to oil spillage must be avoided, not only because it would set a temporarily end to the Arctic activities, but for the sake of protecting the Arctic sea in a sustainable fashion. The latter becomes especially important, because typically the design goal is to minimize cost by fulfilling the minimum required safety margin only.

Consequently, this article seeks to identify the influence of SZT on the crashworthiness of ship side structures and provides the underlying material relation including fractures for different SZTs. Therefore, the material properties of carbon steel subjected to SZT, namely −30, −60 and −90 °C, are obtained experimentally to verify if an increase in load carrying capacity can be expected when such arctic materials are considered. These material properties concern the yield stress, σ_{yield}, the Lüders plateau length, $l_{\text{lüders}}$, the ultimate stress, σ_{ultimate}, and the failure strain, $\varepsilon_{\text{failure}}$, for SZT. Earlier investigations, e.g. ice berg collision simulation, typically neglect the influence of SZT on the material behaviour; see Liu [7]. Hence, this article will show the resulting structural crashworthiness for SZT for standard (std.) materials. These std. materials show a typical increase in yield and ultimate strength as well as Lüders plateau length besides a decrease in fracture strain, with decreasing temperature; see Fig. 1. The resulting energy increase (hatched area for std. material) will thus increase the load carrying capacity of the structure, however, prior to the reduced fracture strain. Hence, if the material could exhibit a further increase in fracture strain at SZT, arctic structures would be safer due to the temperature influence on the material properties. Such arctic material would result in an overall energy increase and load carrying capacity over the entire range of strain; see Fig. 1. Similar findings for basic tensile tests are presented by [8] concerning the general increase in yield and ultimate strength as well as the possibility of an increase in fracture strain. Hence, the experimentally obtained

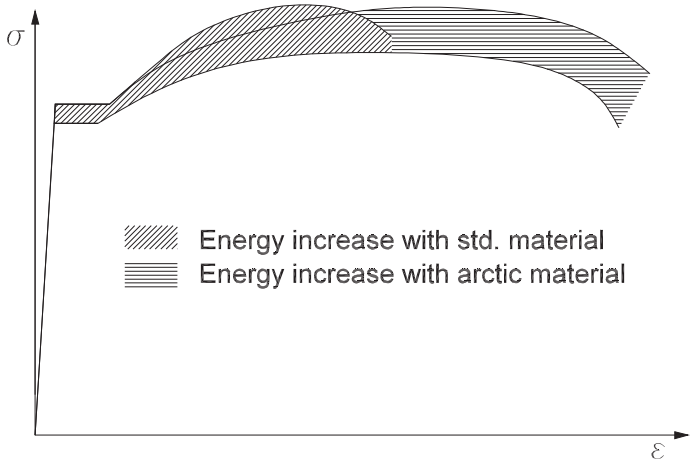

Fig. 1. Influence of sub-zero temperature on the material behaviour.

characteristic material properties obtained in this paper will be mapped on a reliable collision strength assessment method. This will be done in terms of a local strain and stress relation including fracture, which will be used as input for the numerical simulations for different SZTs. Therefore, this article will utilize a method to predict the energy absorbed until fracture of a ship side structure by Ehlers [9]. The reliability of the collision simulations will be achieved, because a consistent link between the local material measurements and the discretized finite element model is obtained on the basis of optical measurements; see Ehlers and Varsta [10] and Ehlers [11]. This consistent link will allow for a sufficiently accurate implementation of fracture initiation and propagation by deleting failing elements at the correct state of strain.

As a result, comparative collision simulations will be carried out for two different structures, which have been tested in large-scale at 10–20 °C. These simulations will serve as a comparative measure to present the theoretical influence of SZT on the collision force. The latter will be achieved by using the different material relationships for SZT. Furthermore, these simulations will identify the potential gain from specially selected materials for SZT, arctic materials, compared to standard materials, both with and without the presence of rupture. Hence, this will identify the potential increase in crashworthiness of structures under SZT and thereby contribute to safe arctic operations and transport.

1.1. The large-scale collision experiments

During the period of 1997–1998 a series of large-scale collision experiments were performed within the EU Crashcoaster project. The experimental setup consisted of an 800 tons inland waterway tanker Nedlloyd 34 striking a 1400 tons inland waterway tanker Amatha with a rigid bow at a 90° angle at 3.33 m/s; see Fig. 2. The test sections were mounted to the struck vessel with a supporting structure. The collision force and the relative ship motions were recorded in the centre of gravity of each ship to derive the force versus penetration curves characterising the structural response. A detailed description of the vessel particulars as well as a discussion on the influence of the test setup on the ship motions and the influence of sloshing can be found in Ehlers et al. [12]. In this paper, two large-scale structures will be analysed numerically to investigate the influence of SZT on the collision force, namely the X-core and a double hull structure.

The laser-welded X-core structure has been designed in the EU Sandwich project [13]. Fig. 3 shows a cross section of the X-core structure. The section consists of four "x" shaped core elements, which are joined by laser welding. The sandwich structure is 360 mm in depth, 1.5 m in height, and 5.5 m in length. The thickness of the outer shell is 6 mm and the X-core and the inner shell thickness is 4 mm and consists of normal shipbuilding steel. Ehlers et al. [12] presents and validates the deformations of

Fig. 2. Large-scale collision experiment [11].

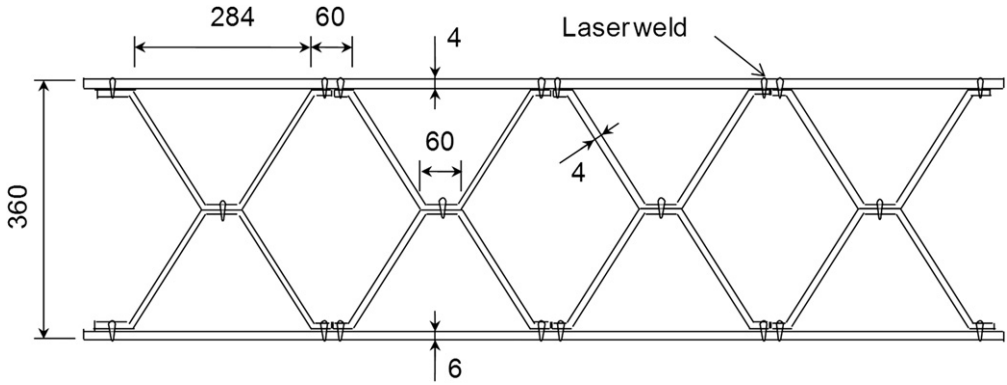

Fig. 3. Cross-section of the X-core structure [11].

the X-core structure, see also Fig. 4, as well as the laser-weld failure based on extensive finite element simulations and a comparison to a digitalized three-dimensional model of the post-experimental structure. Even though the outer plating showed an 18 cm long vertical fracture after the experiment its influence on the force versus penetration curve is neglected in this paper. The latter is well justified based on the insignificant influence on the collision force.

The technical University of Hamburg-Harburg designed the double hull structure; see Peschmann [14]. The simplified test section corresponds to a 35000 DWT tanker in a scale of 1:3 and extends from the deck to the double bottom with a length of 4.5 m; see Fig. 5. The test section consists of normal shipbuilding steel and resulted in a significant rupture of the outer and the inner hull structure; see Fig. 6.

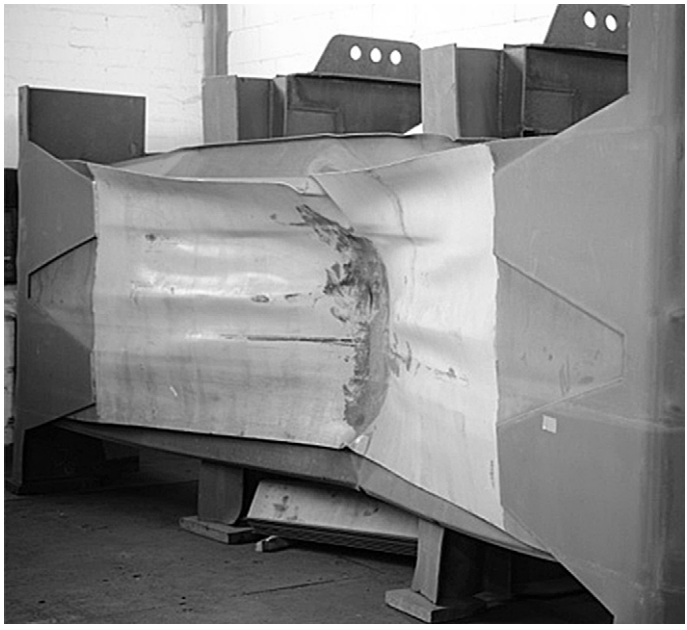

Fig. 4. Post-experimental X-core structure [11].

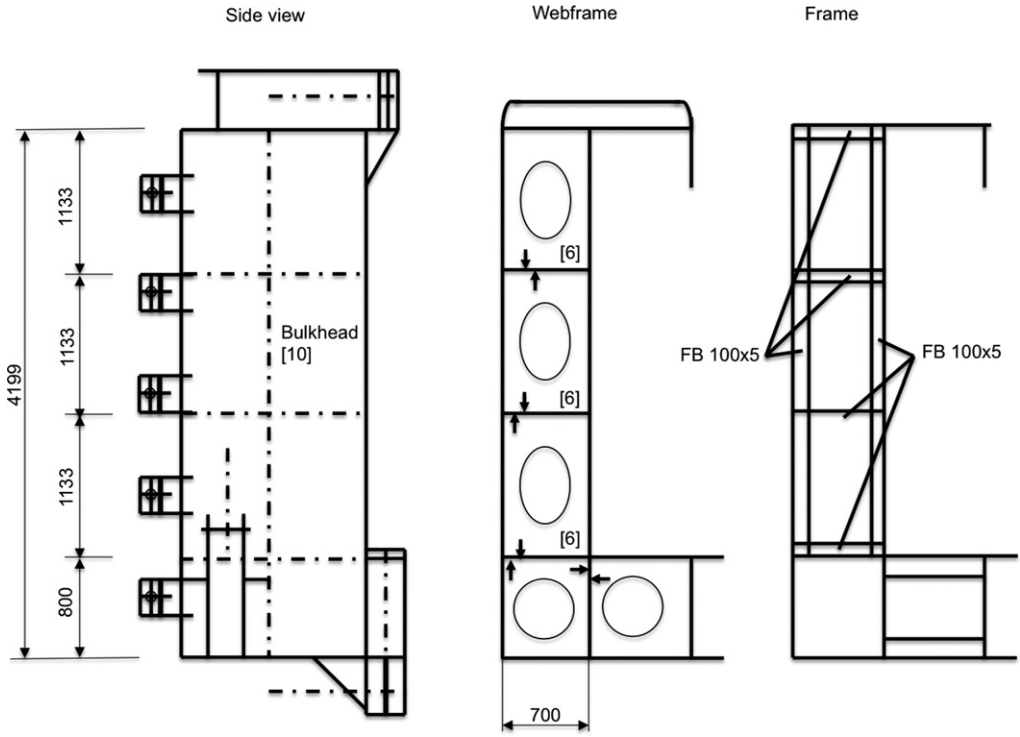

Fig. 5. Double hull side structure according to [13].

Fig. 6. Post-experimental double hull structure [13].

Table 1
Steel chemical composition of the arctic material.

C	Si	Mn	P	S	Cu	Ni	Nb	Ti	Al	N
0.09	0.29	1.43	0.01	0.001	0.01	0.01	0.01	0.013	0.035	0.003

2. Tensile experiments and results for SZT

The motivation of the following SZT experiments arises from the fact that this paper seeks to numerically subject structures previously tested in large-scale under ambient temperatures (10–20 °C) to SZT using material relations for SZT. However, because the large-scale experiments have already been conducted and no base material is available for SZT-testing at this stage, a standard NVA steel material relation for ambient temperatures will be modified in accordance with the characteristic changes under SZT. These characteristic changes are namely the change in σ_{yield}, σ_{ultimate}, $\varepsilon_{\text{failure}}$ and $l_{\text{lüders}}$. Therefore, a series of tensile tests are carried out for 0, −30, −60 and −90 °C.

For the standard NVA steel this paper uses the true strain and stress relationship until fracture for slow displacement speeds, respectively strain rates from 6e-4 to 9e-3, according to [10]. Their measurements have been accomplished at room temperature around 20 °C (20 °C). Furthermore, this element length-dependent NVA material relationship is identified on the basis of optical measurements, where the recordings from the discrete pixel dimensions are mapped onto the discrete finite element length. The Norske Veritas Grade A (NVA) steel is a commonly used shipbuilding steel. Therefore, this material is assumed to represent the material behaviour of the large-scale X-core and

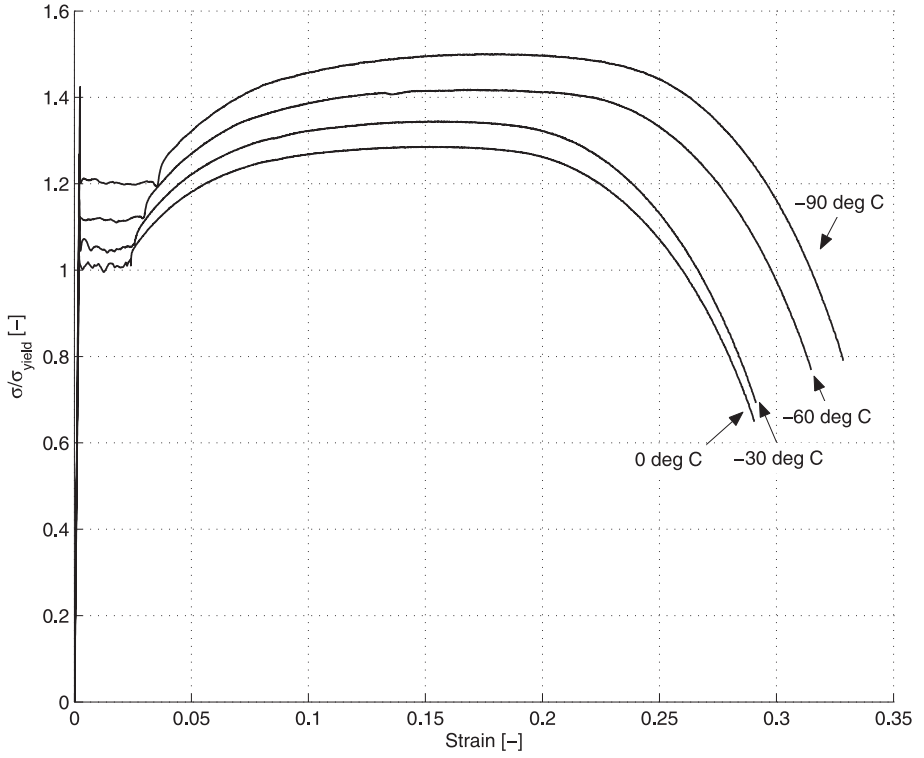

Fig. 7. Normalized tensile test results for SZT.

double side structure at 0 °C. Furthermore, in case of the X-core structure, the laser weld dimension-dependent material behaviour for 20 °C is obtained based on optical measurements; see Jutila [15]. The average width of the laser welds was 1.496 mm. Jutila obtained a normal weld failure force from where the failure stress, $\sigma_{N(\text{weldfailure})}$, equal to 0.947 kN/mm^2, can be found. Jutilas' local surface displacement measurements lead to logarithmic weld failure strain of 0.1. His measurements are in accordance with literature findings; see for example [16,17]. This local weld failure strain is also obtained on the basis of the discrete pixel dimensions from the optical measuring system whereby the strain reference length is clearly defined. This strain reference length is equal to 0.256 mm.

The material suggested as a candidate for Arctic applications is a 355 MPa steel. The base material was delivered as a rolled 50 mm thick plate. The chemical composition of the material is shown in Table 1. Smooth tensile samples with diameter of 10 mm were extracted at the quarter position of the plate thickness transversal to the rolling direction. The testing was performed inside a temperature chamber and thermo couples welded directly onto the specimens were used to control the specimen temperature. A relatively slow displacement was applied resulting in a strain rate of 8e-4 during the testing.

The SZT measurement results are presented in Fig. 7 in terms of normalized global strain and stress curves for the different test temperatures. Consequently, Fig. 8 presents the change in σ_{yield}, σ_{ultimate}, $\varepsilon_{\text{failure}}$ and $l_{\text{lüders}}$ for SZT. Therein, it is very interesting to note that properties increase in value with decreasing temperature. The latter is according to common beliefs a contradiction concerning $\varepsilon_{\text{failure}}$, because for most materials the failure strain decreases with decreasing temperatures as required by DNV [18] for the $\varepsilon_{\text{failure.std}}$. Hence, the resulting local element-length dependent material relations for SZT are obtained using the basic NVA material relation according to Ehlers and Varsta [10] and the characteristic property changes for SZT identified experimentally in Fig. 8. Therein, it can also be seen that only the failure strain is different for both material grades. Additionally, the resulting failure strain versus element length curves for the material with increasing failure strain (arctic material) as well as the standard material (decreasing failure strain) is plotted in Fig. 10 for the different SZTs.

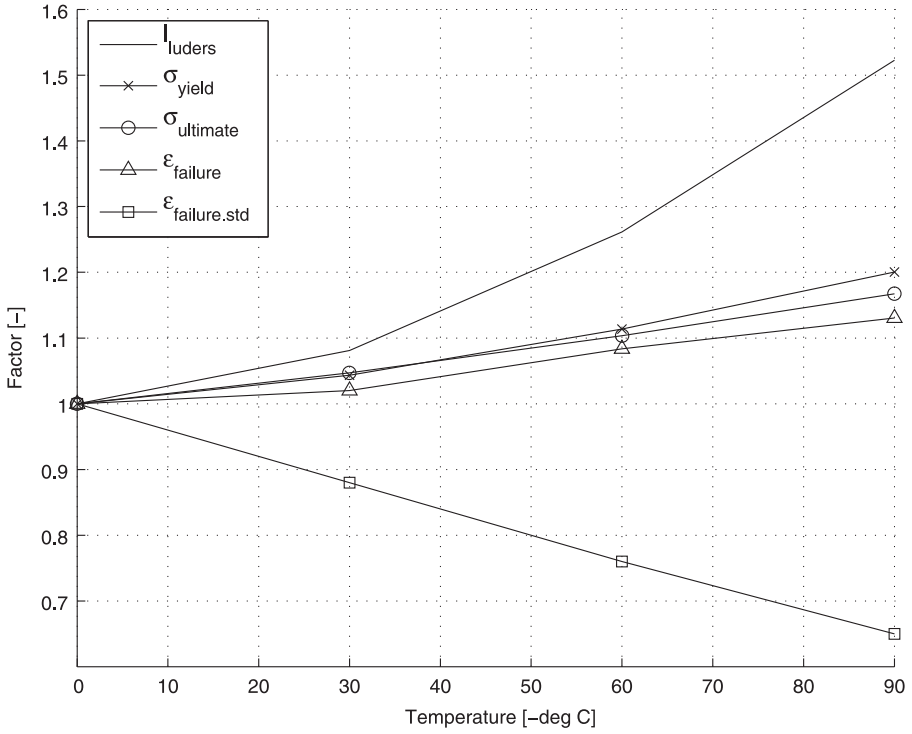

Fig. 8. Change in σ_{yield}, σ_{ultimate}, $\varepsilon_{\text{failure}}$ and $l_{\text{lüders}}$ for SZT.

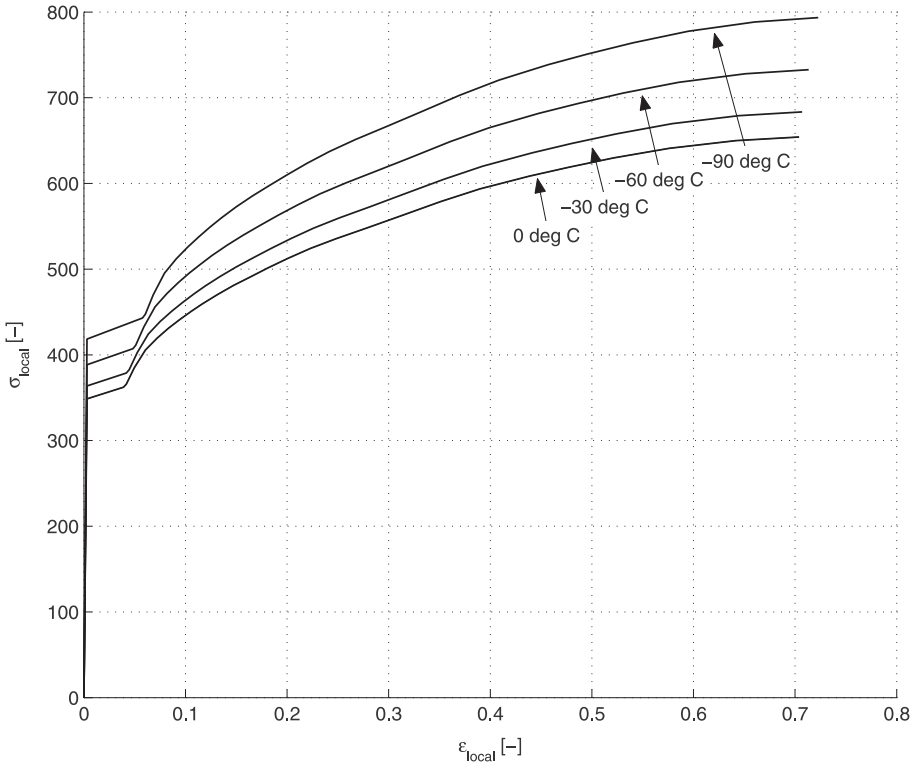

Fig. 9. Local element-length dependent material relations for SZT.

3. Numerical modelling (quasi-static and dynamic)

The explicit solver LS-DYNA version 971 (see Hallquist [19]) is used for the collision simulations. Further, the X-core collision simulations are carried out considering actual ship motions in a coupled approach (D) and prescribed average experimental displacement-controlled motions in a quasi-static (QS) approach. The double hull side structure is solely simulated with prescribed displacement-controlled motions in a QS-approach. The coupled analyses are conducted with the actual velocities and accelerations occurring during the collision while the quasi-static simulations are conducted with a constant prescribed velocity along a pre-defined straight penetration path. Ehlers et al. [12] already presented the influence of the ships motions on the X-core simulations as well as the influence of the laser weld failure. Hence, the focus of the current simulations is the comparison of the resulting force versus penetration curves if the specimens would be subjected to SZT using a standard material and a suitable Arctic material. Therefore, the X-core simulations will highlight this influence in the absence of rupture, whereas the QS-approach used for the double hull structure will further validate this influence in the presence of rupture. The ANSYS parametric design language is used to build the finite element model of both structures using quadrilateral Belytschko-Lin-Tsay shell elements with 4 nodes and five integration points through their thickness. In the contact area, the element length is 4.4 mm, whereas the remaining elements have a length of 26.4 mm in the case of the X-core structure and 33.3 mm and 100 mm for the double hull structure respectively (see Fig. 11). For the coupled approach (D) this paper utilizes the method proposed by Pill and Tabri [20], which allows dynamic collision simulations with LS-DYNA - for modelling details and boundary conditions of the X-core structure

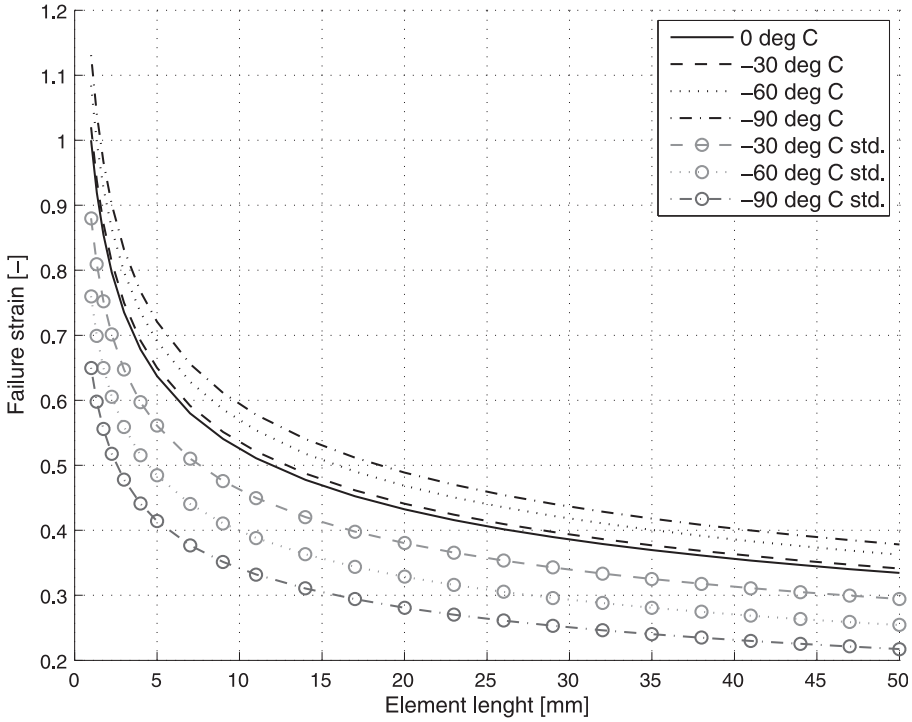

Fig. 10. Failure strain versus element length curves for SZT.

please consult [12]. The boundary conditions of the QS-approach are simple restrictions of all translational and rotational degrees of freedom at the longitudinal cross-sections at each end of the specimen. Standard LS-DYNA hourglass control is used for the simulations. The automatic single surface contact of LS-DYNA is used to treat the contact. The static friction coefficient was assumed to be 0.3.

3.1. Material modelling and weld modelling

The failure strain and element length relationship presented in Figs. 9 and 10 is implemented in the ANSYS parametric design language model generation via material 24 of LS-DYNA [19], which allows failing elements to be removed at the critical strain. This constant strain failure criterion is justified due to the close ranges of triaxiality at failure for thin plates [9]. The strain rate sensitivity is not included in this material relationship, as no influence on the ultimate tensile force and failure strain for different displacement speeds are found; see [12].

The constraint spot weld model of LS-DYNA [19] is used to represent the laser weld of the X-core structure. Therefore, the gap between the X-core structures steel plates is set to 0.256 mm and is used to represent the laser weld with a weld failure strain of 0.1. This failure strain is assumed to follow the same trend as indicated in Fig. 8 for SZT. Early simulations by Ehlers et al. [12] showed that less than 1% of the constraints fail due to the failure force and therefore this adjustment is neglected in this analysis. Furthermore, there were 10,305 spot welds, or 227 spot welds per meter of laser weld, which are considered sufficiently dense to represent a continuous laser weld. Furthermore, the choice of the constraint spot weld model is justified as it assumes that the massless spot weld is torn out of the adjacent plates once the critical state is reached. This behaviour is in line with the experimental observations of the laser weld failure; see [12].

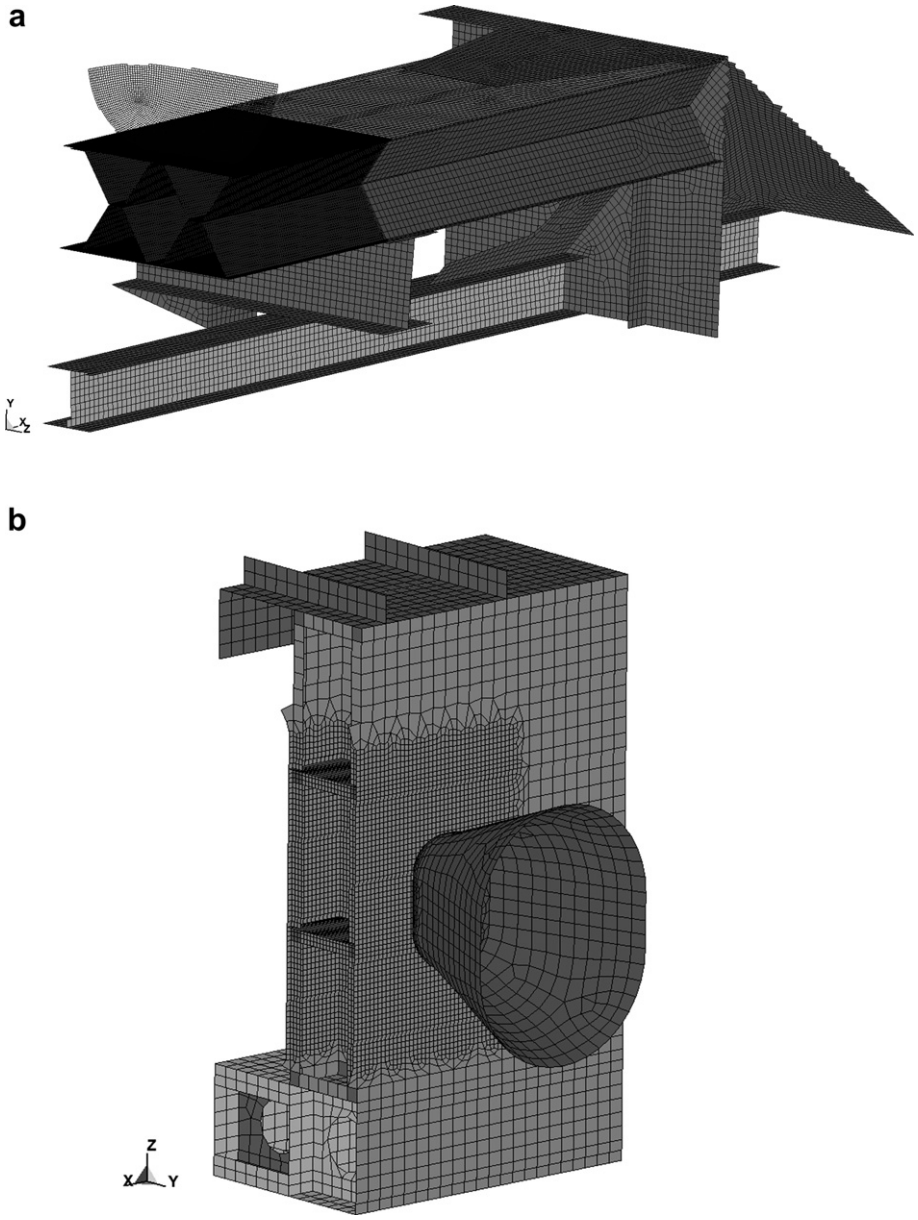

Fig. 11. A quarter of the finite element model of the X-core structure (a) and half of the double hull structural model (b).

4. Collision simulation results for SZT

The resulting force versus penetration curve for the X-core (QS and D) and double hull (QS) structure are shown in Figs. 12 and 13, respectively, together with the experimental results for comparison.

The collision simulations of the X-core structure for zero degrees Celsius (0 °C) comply sufficiently well with the experimental results, especially if the significant noise in the experimental signal is considered and the fact that penetration is derived from the actual ship motions. A detailed discussion

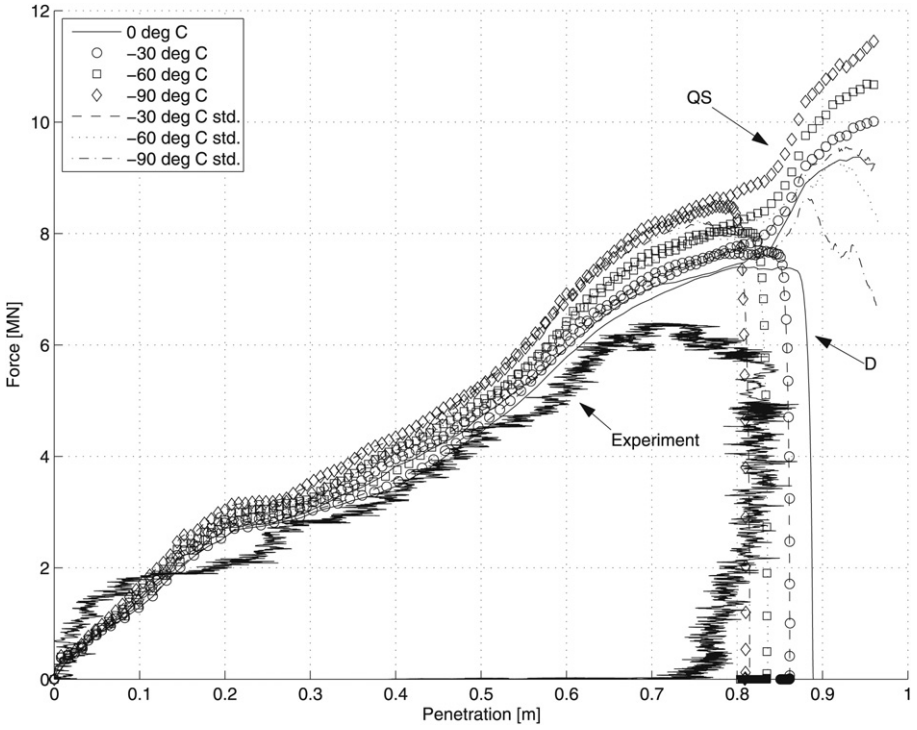

Fig. 12. X-core collision simulation results for SZT.

on the compliance and influences at ambient temperature can be found in [12]. Furthermore, simulations using a standard material (std.) and the arctic material correspond well to one another for the different SZT, both for the QS and D simulations, see Tables 2 and 3. Obviously, only the D simulations are able to simulate the separation of the vessels as a result of the absorbed collision energy, and thus they visualize the reduction in penetration depth with decreasing temperatures as well as the increase in collision force. The latter occurs, because more energy can be absorbed for the same level of deformation compared to 0 °C prior to rupture, see also Fig. 1. Additionally, the QS simulations show the continuation of the force penetration curve and thereby the subsequent drop in force as a result of outer shell rupture initiation for the 0 °C curve. Thus, this behaviour is well in line with the experimental observation of an 18 cm long rupture in the outer shell at the end of the experiments. Furthermore, for lower temperatures the std. material follows this drop in force, whereas the arctic material is continuously able to increase the collision force as a result of the increase in fracture strain according to Fig. 1.

The significant influence of rupture occurrence on the collision force for SZT is clearly visible for the double hull simulations show in Fig. 13. The 0 °C simulation corresponds sufficiently well to the experimental results concerning the overall trend and the coarsely meshed model; see also Table 4. The outer and inner hull rupture ($r_{\text{outer-shell}}$ and $r_{\text{inner-shell}}$) is clearly seen by the force peaks. Furthermore, the opposite trend in force prediction for the std. and arctic material due to the opposite fracture strain behaviour, see Fig. 8, is clearly visible and results in a significant difference. The std. material reduces the collision force of up to 21% compared to the increase for the arctic material up to 33% for the outer hull peak force. Thus, the std. material is able to absorb significantly less energy during such collision event and the resulting damage is comparably larger. The structure build with the arctic material is however able to absorb significantly more energy due to the increased energy absorption capacity of the material, see also Fig. 1.

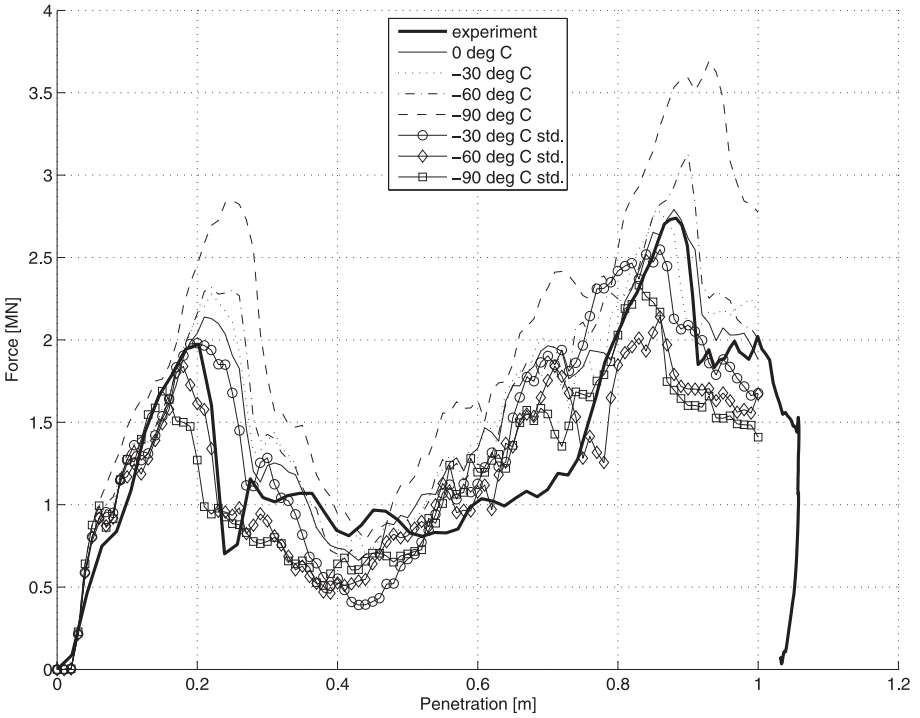

Fig. 13. Double hull structure collision simulation results for SZT.

5. Discussion

The presented collision simulations clearly show the influence of SZT on the collision force for standard material, decreasing fracture strain for decreasing temperature, and arctic material, increasing fracture strain for decreasing temperature. The ratio of simulate forces for SZT compared to 0 °C is presented in Fig. 14a Therein, it can be clearly seen that the increase in σ_{yield}, $\sigma_{ultimate}$ and $l_{lüders}$ following Fig. 8 results in gain in collision force of up to 15%, see Fig. 14b, in the absence of fracture. Hence, the arctic material performs equally well in terms of increased collision force as the std.

Table 2
Maximum force prediction (QS) for the X-core structure ($F_{max\_experiment}$ occurs at a penetration of 0.725 m).

		Experiment	
F_{max} [kN]		6.39	7.23
$F/F_{max\_experiment}$		1	1.14
$F/F_{max\_0°}$		0.88	1
Arctic material	−30 °C	−60 °C	−90 °C
F_{max} [kN]	7.43	7.82	8.28
$F/F_{max\_experiment}$	1.16	1.22	1.30
$F/F_{max\_0°}$	1.03	1.08	1.15
Std. material	−30 °C	−60 °C	−90 °C
F_{max} [kN]	7.38	7.75	8.17
$F/F_{max\_experiment}$	1.15	1.21	1.28
$F/F_{max\_0°}$	1.02	1.07	1.13

Table 3
Maximum force prediction (D) for the X-core structure.

		Experiment	0 °C
F_{max} [kN]		6.39	7.01
$F/F_{max\_experiment}$		1	1.09
$F/F_{max\_0^\circ}$		0.91	1
Arctic material	−30 °C	−60 °C	−90 °C
F_{max} [kN]	7.29	7.69	8.2
$F/F_{max\_experiment}$	1.14	1.20	1.28
$F/F_{max\_0^\circ}$	1.04	1.10	1.16
Std. material	−30 °C	−60 °C	−90 °C
F_{max} [kN]	7.29	7.68	8.06
$F/F_{max\_experiment}$	1.14	1.20	1.26
$F/F_{max\_0^\circ}$	1.04	1.10	1.15

material. Additionally, no sensitivity to the weld failure was found for the X-core structure for SZT, thus confirming the earlier findings from Ehlers et al. [12]. However, Ehlers et al. also presents a significant decrease in force for very low weld failure strains. The latter indicates that in case the laser weld would behave very brittle for SZT, than this would influence the collision force. However, further research of laser weld failure under SZT will be needed to investigate this influence. Concerning the double hull structure, it is assumed that SZT will not cause a transition to an unstable fracture mode, because the stress triaxiality due to the small plate thickness is found to be low, besides the increasing fracture strain at SZT of the base material. However, for a standard material unstable fracture may occur due to the decreasing fracture strain at SZT of the base material. The latter requires further investigations, which are left for future work however.

Nonetheless, the gain in collision force using arctic material already increases compared to a standard material to a significant extend in the presence of rupture as shown for the double hull simulations. Therein, the gain in collision force is up to 55% and thus outlining the necessity to select the material accordingly, respectively with increased failure strain for SZT, see Fig. 14b. Furthermore, this increased energy absorption capacity at SZT indicates a decrease in damage extent and thereby repair cost analogously to the use of high strength steel in crashworthy side structured presented by Ehlers [21].

Table 4
Maximum force and displacement predictions (QS) for the double hull structure.

		Experiment	0 °C
$F_{outer\text{-}shell}$ [MN]		1.97	2.13
$r_{outer\text{-}shell}$ [m]		0.2	0.21
$F_{inner\text{-}shell}$ [MN]		2.73	2.79
$r_{inner\text{-}shell}$ [m]		0.89	0.88
Arctic material	−30 °C	−60 °C	−90 °C
$F_{outer\text{-}shell}$ [MN]	2.27	2.31	2.84
$r_{outer\text{-}shell}$ [m]	0.22	0.22	0.25
$F_{inner\text{-}shell}$ [MN]	2.82	3.12	3.59
$r_{inner\text{-}shell}$ [m]	0.86	0.89	0.9
Std. material	−30 °C	−60 °C	−90 °C
$F_{outer\text{-}shell}$ [MN]	1.98	1.84	1.69
$r_{outer\text{-}shell}$ [m]	0.2	0.18	0.15
$F_{inner\text{-}shell}$ [MN]	2.55	2.33	2.01
$r_{inner\text{-}shell}$ [m]	0.86	0.83	0.83

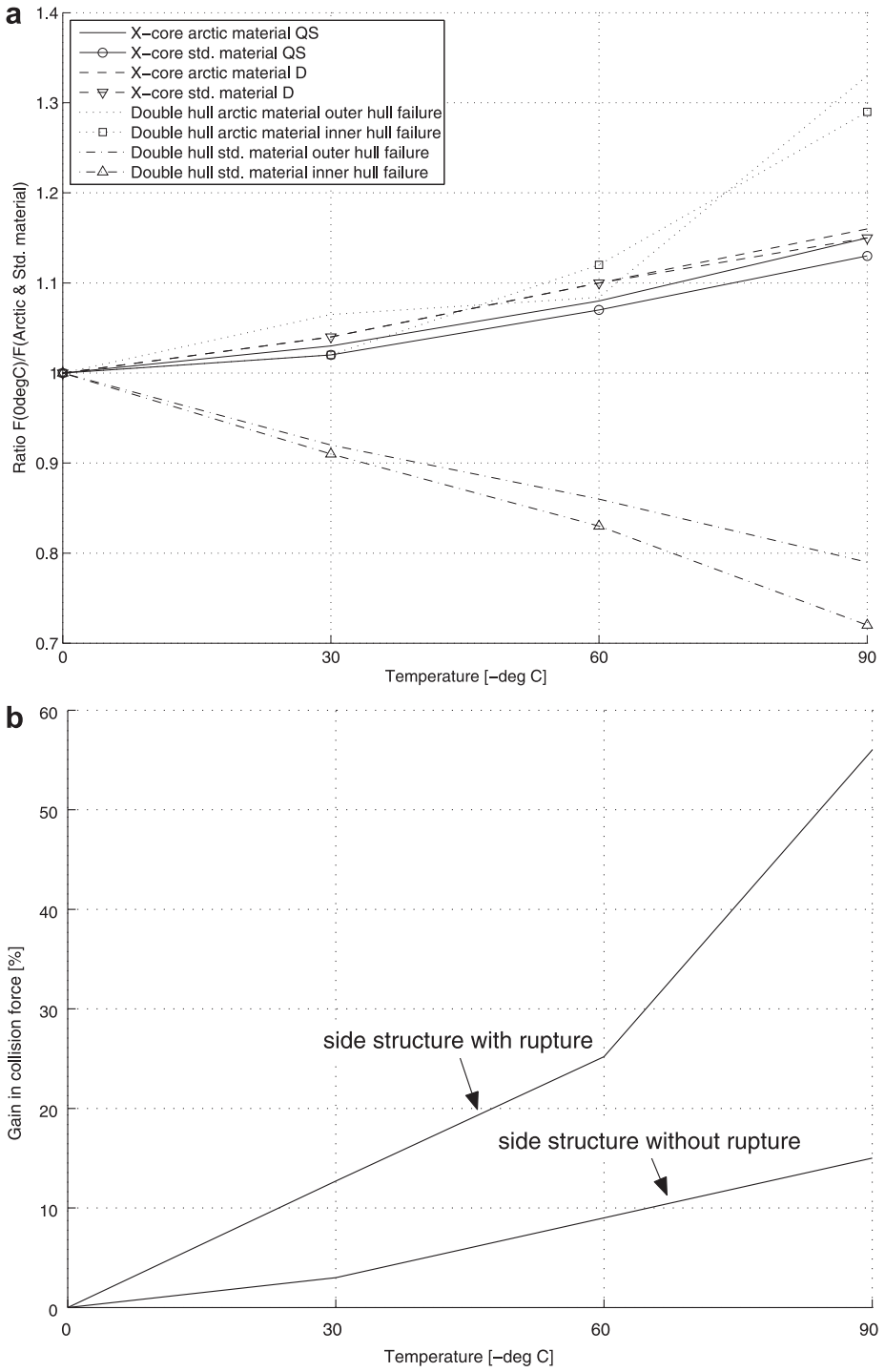

Fig. 14. Collision force comparison (a) and resulting gain in collision force (b) for the arctic material.

6. Summary

Arctic conditions, respectively sub-zero temperatures, increase the structural safety level in accidental events, such as collisions, due to the higher energy absorption capacity of the material. Both, steel grades increase the collision force, respectively energy absorption capacity, for the simulated structures as a result of SZT due to the increase in σ_{yield}, $\sigma_{ultimate}$ and $l_{lüders}$. Hence, prior to rupture SZT increase the collision resistance and further, if a suitable material is chosen, which exhibits an increase in fracture strain for decreasing temperatures, an additional gain of up to 30% in collision force can be achieved.

Acknowledgements

The financial support of the Norwegian Ministry of Trade and Industry is highly acknowledged.

References

[1] DNV. Shipping across the Arctic Ocean - A feasible option in 2030–2050 as a result of global warming?. Position Paper 04–2010; 2010.
[2] IMO. International Maritime Organisation. Casualty statistics and investigations: very serious and serious casualties for the year 1999. FSI.3/Circ.2, 2001; Available at: http://www.imo.org/includes/blastDataOnly.asp/data_id%3D5397/2.pdf; 1999 [accessed 04.08.08.].
[3] IMO. International Maritime Organisation. Casualty statistics and investigations: Very serious and serious casualties for the year 2000. FSI.3/Circ.3, 2002; Available at: http://www.imo.org/includes/blastDataOnly.asp/data_id%3D5118/3.pdf; 2000 [accessed 04.08.08.].
[4] IMO. International Maritime Organisation. Casualty statistics and investigations: very serious and serious casualties for the year 2001. FSI.3/Circ.4, 2004; Available at: http://www.imo.org/includes/blastDataOnly.asp/data_id%3D8934/4.pdf; 2001 [accessed 04.08.08.].
[5] IMO. International Maritime Organisation. Casualty statistics and investigations: very serious and serious casualties for the year 2002. FSI.3/Circ.5, 2005; Available at: http://www.imo.org/includes/blastDataOnly.asp/data_id%3D11539/5.pdf; 2002 [accessed 04.08.08.].
[6] IMO. International Maritime Organisation. Casualty statistics and investigations: very serious and serious casualties for the year 2003. FSI.3/Circ.6, 2005; Available at: http://www.imo.org/includes/blastDataOnly.asp/data_id%3D11540/6.pdf; 2003 [accessed 04.08.08.].
[7] Liu Z. Analytical and numerical analysis of iceberg collisions with ship structures. Doctoral thesis, Norwegian University of Science and Technology; 2011.
[8] Paik S, Kim BJ, Park DK, Jang BS. On quasi-static crushing of thin-walled steel structures in cold temperature: experimental and numerical studies. International Journal of Impact Engineering 2011;38:13–28.
[9] Ehlers S. A procedure to optimize ship side structures for crashworthiness. Journal of Engineering for the Maritime Environment 2010a;2010(224):1–12.
[10] Ehlers S, Varsta P. Strain and stress relation for non-linear finite element simulations. Thin-Walled Structures 2009;47:1203–17.
[11] Ehlers. The influence of the material relation on the accuracy of collision simulations. Marine Structures 2010b;2010(23):462–74.
[12] Ehlers S, Tabri K, Romanoff J, Varsta P. Numerical and Experimental Investigation on the collision resistance of the X-core structure. Journal of Ships and Offshore Structures 2010;7(1):21–9.
[13] Wolf M. Full scale collision experiment, X-type Sandwich side hull. EU Sandwich Project Report Deliverable TRD448; 2003. 21 p..
[14] Peschmann J. Energy absorption computations of ship steel structures under collision and grounding (translated from German). Doctoral Dissertation. Technical University of Hamburg; 2001.
[15] Jutila M. Failure mechanism of a laser stake welded T-joint. Master of Science Thesis. Helsinki University of Technology. Department of Applied Mechanics; 2009.
[16] Çam G, Erim S, Yeni Ç, Koçak M. Determination of Mechanical and fracture properties of laser Beam welded steel joints. Supplement to the Welding Journal; June 1999:193s–201s.
[17] Borońsk D. Cyclic material properties distribution in laser-welded joints. International Journal of Fatigue 2006;28:346–54.
[18] DNV. Offshore standard DNV-OS-B101. Metallic Materials; April 2009.
[19] Hallquist JO. LS-DYNA keyword user's manual. Version 971. California: Livermore Software Technology Cooperation; 2007.
[20] Pill I, Tabri K. Finite element simulations of ship collisions: a coupled approach to external dynamics and inner mechanics. In: Proceedings of analysis and design of marine structures; 2009. p. 103–9.
[21] Ehlers S. A particle swarm algorithm-based optimization for high-strength steel structures. Journal of Ship Production and Design 2012;28(1):1–9.